Microstructural study of very low resistivity TiN_x films formed by rapid thermal low-pressure metalorganic chemical vapour deposition on InP

1993 Semicond. Sci. Technol. 8 450

(http://iopscience.iop.org/0268-1242/8/3/026)

Semicond. Sci. Technol. 8 (1993) 450–458. Printed in the UK

Microstructural study of very low resistivity TiN_x films formed by rapid thermal low-pressure metalorganic chemical vapour deposition onto InP

A Katz†, A Feingold†, S Nakahara†, S J Pearton†, E Lane† and K Jones‡

†AT&T Bell Laboratories, Murray Hill, NJ 07974-0636, USA
‡University of Florida, Gainesville, FL 32601, USA

Received 13 July 1992, accepted for publication 29 September 1992

Abstract. Significant reductions in sheet resistivity of TiN_x films formed by rapid thermal low-pressure metalorganic chemical vapour deposition onto InP, were realized by increasing the substrate temperature through the deposition, utilizing a post-deposition, *in situ*, heat treatment at temperatures up to 600 °C, and adding tertiarybutylphosphine (TBP) metalorganic precursor to the reactive gas mixture. As a result, film resistivity values as low as 30 $\mu\Omega$ cm were obtained. Extensive transmission electron microscopy analysis was performed and the formation of a new and unidentified phase, having a similar crystal structure and lattice constant to those of $Li_9TiN_2O_2$, was identified. This phase was formed as a result of TiN_x–P intermixing during high-temperature post-deposition sintering of the TiN_x/InP system, or as a result of incorporating P in the deposited TiN_x film by bleeding TBP. This phase formation is likely to be the origin of the observed reduction in film resistivity.

1. Introduction

The excellent mechanical and thermal stability of TiN_x films, in addition to its high conductivity, have made it one of the most attractive contact and diffusion barrier metallization candidates in microelectronic device fabrication [1–4].

TiN_x films have been deposited by various physical [5, 6] and chemical [7, 8] deposition techniques, with the latter allowing for the realization of two attractive properties, namely an excellent conformal step coverage and selective deposition on semiconductor materials over dielectric layers [9]. Among the chemical deposition techniques for TiN_x films to III V semiconductor material, rapid thermal low-pressure metalorganic chemical vapour deposition (RT-LPMOCVD) was found to be of special interest [10–12], in particular due to the degradation-free metal/semiconductor interface achieved as a result of the rapid film deposition process driven by the halogen-tungsten lamp heating pulse.

RT-LPMOCVD of the TiN_x film, carried out using Tetrakis (dimethylamido) titanium (DMATi) and ammonia as the reactive precursors in the gas mixture yielded a stoichiometric, high-quality film structure, which contained, however, about 20% of impurities such as carbon and oxygen, resulting in a very high resistivity.

The purpose of this work was to apply some procedures, such as an *in situ* post-deposition sintering process, and enrichment of the reactive gas mixture by adding tertiarybutylphosphine (TBP), in an attempt to reduce the concentration of the entrapped impurities, and thus improve the film conductivity.

2. Experimental procedure

TiN_x films were deposited onto (100) InP by the RT-LPMOCVD technique using an A G Associates Heatpulse CVD-800™, which has been described in detail elsewhere [13]. The wafers were deoxidized in 10:1 H_2O:HF solution and subsequently degreased by being rinsed in warm chloroform, acetone and methanol, prior to being loaded into the CVD-800™ load-lock chamber. This chamber was pumped down to a pressure of 9×10^{-6} Torr in 15 s.

0268–1242/93/030450 + 09 $07.50

The American Cyanamid Tetrakis (dimethylamido) titanium (DMATi) Cypure™ product, loaded in a standard 100 g stainless-steel bubbler, was used as the metal-organic precursor for the TiN_x. Ultra high-purity H_2, passed through a Nanochem gas-purifying system was used as a carrier gas for the TiN_x precursor and as a diluent for the gas mixture, which also contained Matheson electronic grade ammonia (NH_3). TBP was added to the gas mixture in some of the deposition cycles in an attempt to explore the influence of the entrapped phosphine on the properties of the deposited film. The gas mixture was flowed into the chamber over the loaded cold substrate for at least 2 min before turning the lamps on at the end of the deposition cycle. The deposition conditions were as follows: the chamber pressure was varied in the range of 3 to 10 Torr, the temperature was kept in the range of 350 to 400 °C and the $H_2:NH_3$:DMATi ratio in the gas mixture was kept as 125:1:10, with an addition of 1-10 parts of TBP in some of the runs.

An *in situ*, post-deposition sintering cycle at elevated temperatures up to 600 °C was applied to some of the wafers under an H_2 atmosphere, prior to unloading the sample. In all the deposition cycles the substrates were allowed to cool down in the reactor under a H_2 flow for 2 min before unloading to the load-lock.

Various analytical techniques were used to characterize the properties of the RT-LPMOCVD TiN_x films. Scanning electron microscopy (SEM) and transmission electron microscopy (TEM), in both cross-sectional and plan-view modes were used to study the film morphology and microstructure, as well as the nature and extent of the metal–semiconductor interfacial reactions. Auger electron spectroscopy (AES) with sputter depth profiling was carried out to determine the stoichiometry of the TiN_x layers and the composition of the metal–semiconductor interfaces. *In situ* stress measurements were performed using the Flexus 2-300S thin-film stress measurement system. The deposited film thicknesses were measured using a Dektak™ stylus profilometry system and were verified by SEM cross-sectional analysis. The electrical properties of the films were measured by a four-point probe system.

Dry etching of the RT-LPMOCVD films was carried out with either SF_6/O_2, CF_4/O_2 or CHF_3/O_2 discharges contained within an hybrid electron cyclotron resonance (ECR)/radio frequency (RF) system, using an AZ1330J photoresist mask on the TiN_x films.

3. Results and discussion

3.1. Influence of the deposition temperature and post-deposition sintering temperature on the TiN_x microstructure

In previous work we have discussed in detail the properties of TiN_x films that were grown by RT-LPMOCVD from a gas mixture which comprised H_2,NH_3 and DMATi [12]. Deposition rates of 1 to 3 nm s^{-1} at total chamber pressures in the range of 2 to 10 Torr and temperatures of 300 to 350 °C at a NH_3:DMATi flow rate ratio of 1:2 to 1:15 were achieved for these films. Stoichiometric film compositions were obtained, with carbon and oxygen impurity concentrations as low as 5% and 10%, respectively. The AES profile of a representative film is shown in figure 1(*a*). A major concern with this type of TiN_x film is, in particular, the high concentration of the oxygen, which dictates a relatively high film resistivity and thus high resistivity of the resultant contacts. It was concluded, however, that with the given reactor geometrical design and the given reactive chemistry, the film impurity entrapment, as is reflected in the AES (see figure 1(*a*)), cannot be further reduced.

As an attempt to reduce the entrapped oxygen concentration, sintering cycles at various temperatures from 300 to 600 °C for durations of 30 s, were applied to the samples immediately subsequent to the TiN_x film deposition, while still in the chamber. As a result, an intermixed interface between the TiN_x and InP was formed. A noticeable ternary interaction occurred between the Ti, N and P elements in the original TiN_x film volume. This was associated with a sharp reduction of the O concentrations in the deposited films for sintering at temperatures higher than 425 °C, as can be seen in figures 1(*b*) and 1(*c*).

TEM analyses of plan-view samples were carried out in order to identify the formation of new phases as a result of this ternary metallurgical interreaction. Figure 2 shows TEM plan-view selected-area electron diffraction patterns taken from samples that were deposited at 350 °C for 15 s (figure 2(*a*)) and subsequently sintered at various temperatures of 415 (figure 2(*b*)), 500 (figure 2(*c*)) and 550 °C (figure 2(*d*)). All the diffractions were taken from fields that were 73 K magnified, with an acceleration voltage of 200 kV, a camera length of 82 cm, and a

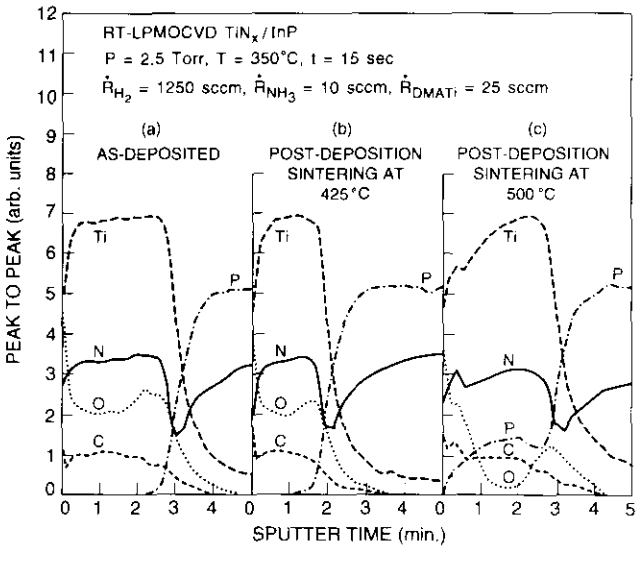

Figure 1. AES depth profiles of TiN_x/InP system (*a*) as-deposited, and after post-deposition *in situ* sintering at temperatures of (*b*) 425 °C and (*c*) 500 °C for 30 s.

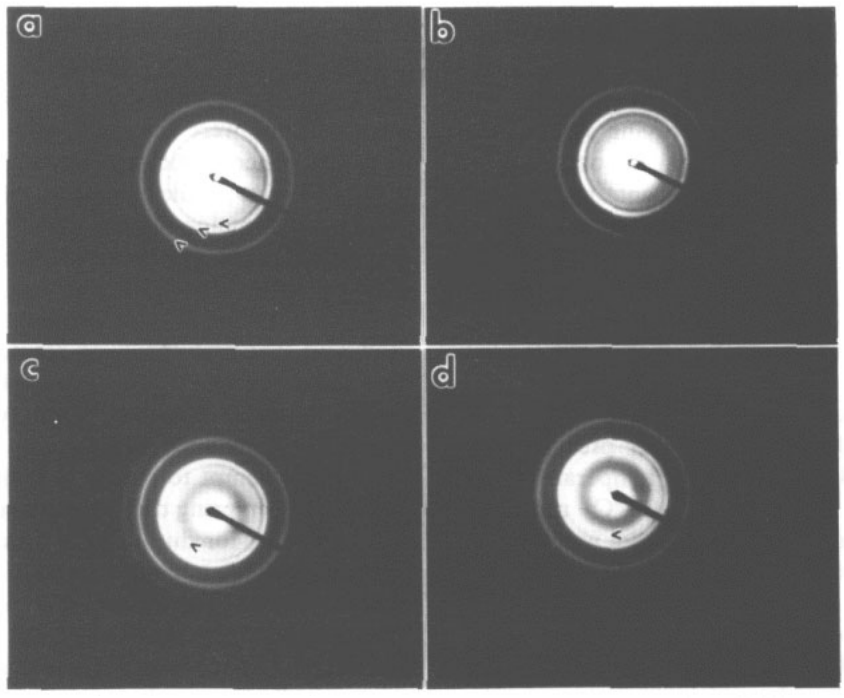

Figure 2. Selected area diffraction patterns of the TiN_x film deposited at 350 C onto InP: (*a*) as-deposited (the J FCC TiN phase rings are marked), and after post-deposition sintering at (*b*) 415 °C and (*c*) 500 °C (the newly formed unidentified phase ring is marked) and at (*d*) 550 °C (the newly formed unidentified phase ring is marked).

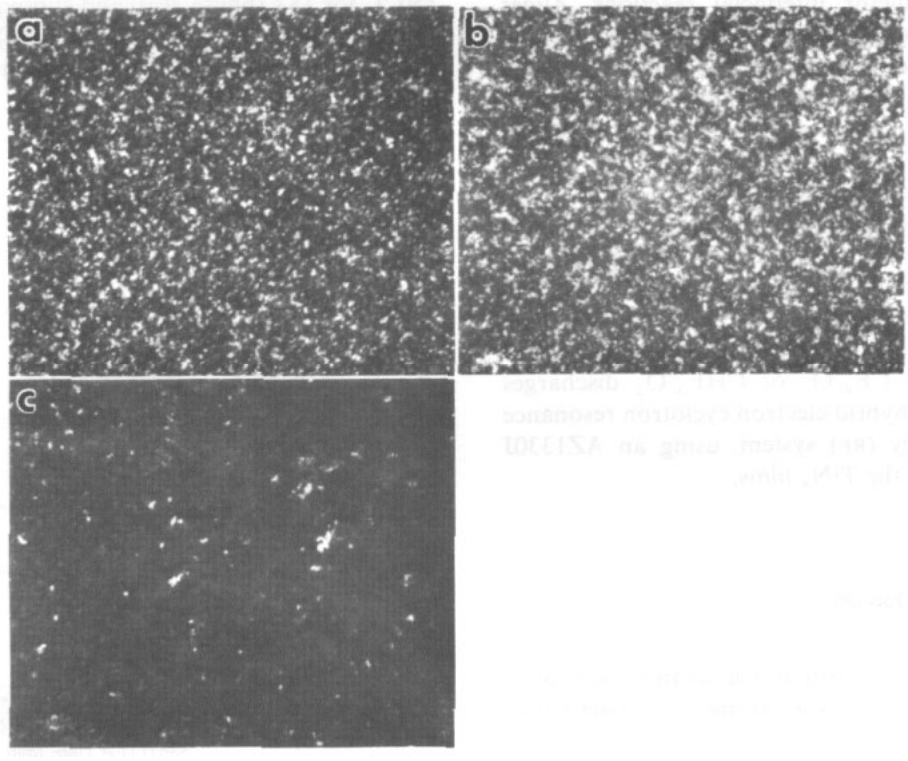

Figure 3. TEM plan-view centred dark-field micrographs of the TiN_x film deposited at 350 °C onto InP: (*a*) as-deposited, taken from *g*111 of the J FCC TiN phase ring, and after post-deposition sintering at 550 °C, taken from (*b*) *g*111 of the J FCC TiN phase ring, and (*c*) the first ring of the unidentified phase.

camera constant (λL) of 2.05 cm Å. The only phase that was identified at the as-deposited TiN_x film and after sintering at 415 °C was the standard, J FCC phase of TiN. Upon annealing at higher temperatures, the InP/TiN reaction yielded a new phase that could not have been identified from the x-ray (JCPDS) file searcher. This new observed phase, the rings of which are marked in figures 2(*c*) and 2(*d*), has a crystal structure and lattice constant similar to the identified $Li_9TiN_3O_2$ phase. The fact that the unknown phase was not discernible in samples that were sintered at temperatures lower than 415 °C may simply be a result of an insufficient quantity of the new phase to yield enough diffraction to be observed, and not due to the fact that it was not formed at this temperature. The structure and characterization of this phase are currently under further investigation. Figure 3 shows centred dark fields of the as-deposited TiN film, taken from *g*111 of the J phase (figure 3(*a*)), of the TiN/InP sample after sintering at 550 °C, taken from the *g*111 of the J phase (figure 3(*b*)) and from the first (marked) ring of the unidentified phase (figure 3(*c*)). One can see that the annealing did not markedly change the grain size of the TiN phase (20–50 Å diameter). A more defined orientation of the new unidentified phase grain is observed, however, for increases in the post-deposition heating temperature to 550 °C or higher.

A chemical analysis of the new phase grains, carried out by means of the TEM-EDAX technique, suggested that it is a ternary phase, comprising about 10% of P in addition to Ti and N. This observation is verified, as well, by the AES results, previously discussed (see figure 1), which clearly showed a Ti–N–P ternary layer formation at the original TiN_x–InP interface, as a result of sintering at temperatures higher than 400 °C.

Further evidence of the interfacial reaction at the TiN_x–InP interface which leads to the formation of the new and unidentified Ti–N–P phase, was provided by investigating the influence of the TiN_x film deposition temperature on the film structure. Figure 4 shows the TEM bright-field images and selected-area electron diffraction patterns of the TiN_x films deposited onto InP substrates that were heated to various temperatures of, for example, 350 (figure 4(*a*)), 400 (figure 4(*b*)) and 450 °C (figure 4(*c*)). The same new ternary phase, discussed earlier, was identified in the as-deposited TiN_x films that were deposited at temperatures of 400 °C or higher. AES of these films revealed evidence of out-diffusion of P from the InP substrate into the TiN_x layer when the deposition took place at these high temperatures. Applying post-deposition sintering led to reorientation of the new-formed phase when carried out at the same or higher temperature than the deposition temperature. Figure 5 shows the TEM bright-field image and selected-area diffraction pattern of the TiN_x film that was deposited onto InP at 400 °C and post-deposition sintered at 450 °C for 30 s. One can see that a reorientation of the as-deposited new unidentified phase (see figure 4(*c*)) took place as a result of the heating.

The influence of the film microstructure evolution through the post-deposition sintering cycles on their

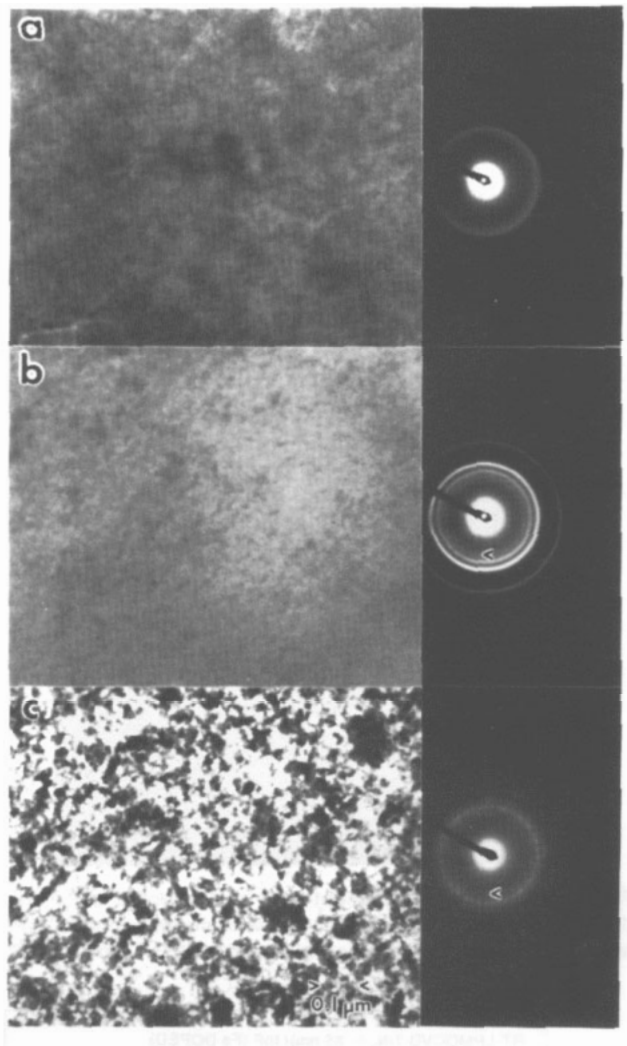

Figure 4. TEM bright-field images and selected-area diffraction patterns of TiN_x films deposited onto InP for 15 s at various temperatures: (*a*) 350 °C, (*b*) 400 °C and (*c*) 450 °C. The marked rings are associated with a newly formed unidentified phase.

electrical properties was evaluated by means of film resistivity measurements. Plot 1 of figure 6 gives the resistivity of TiN_x film that was deposited at 350 °C, as a function of the post-deposition sintering temperature. A significant reduction is observed in this parameter from the as-deposited value of 4×10^4 $\mu\Omega$ cm to about 220 $\mu\Omega$ cm as a result of heating the samples after deposition. In particular, the resistivity drops sharply as a result of sintering at temperatures of 400 °C or higher, which correlates with the film microstructural changes that were observed as a result of heating at this temperature. Moreover, the etch rates of the TiN_x in the ECR-RF discharges described earlier also showed similar decreases to the resistivity, indicating the presence of microstructural changes. For post-deposition sintering at temperatures above 600 °C, the TiN_x would not etch at all.

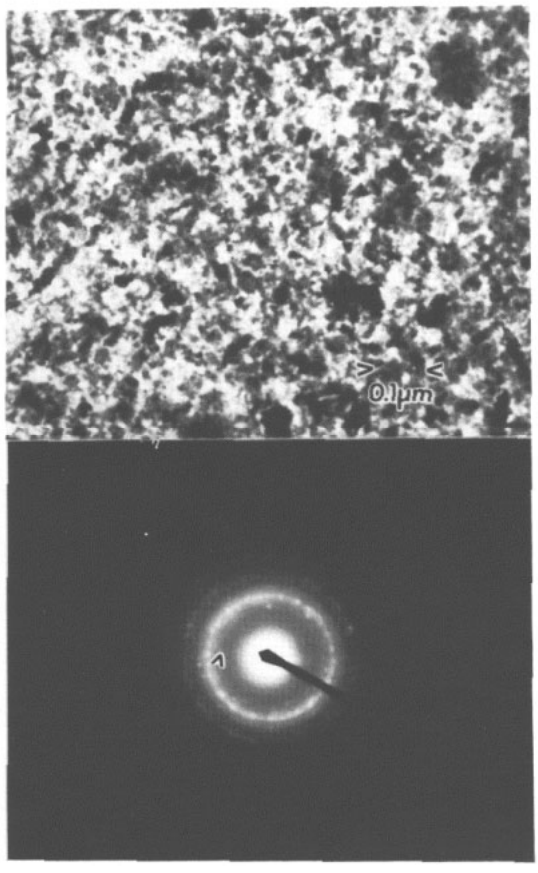

Figure 5. TEM plan-view bright-field and selected electron diffraction pattern of TiN_x film that was deposited onto InP at 400 °C and post-deposition sintered at 450 °C for 30 s.

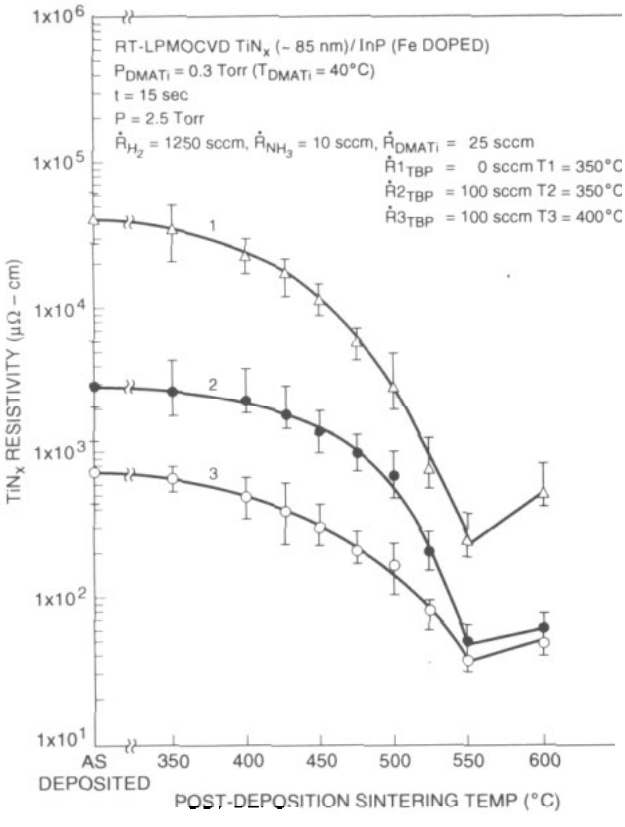

Figure 6. Film resistivity as a function of post-deposition sintering temperature, the amount of TBP in the mixed reactive gas and the deposition temperature.

3.2. Influence of adding phosphorus to the reactive gas mixture on the properties of the deposited film

Since the desired reduction of the TiN_x film resistivity was attributed to the Ti-N-P reaction driven by the post-deposition sintering which led to out-diffusion of P into the TiN layer, an attempt was made to purposely introduce free phosphorus atoms into the as-grown film. The phosphorus atoms were provided by adding the TBP liquid metalorganic precursor to the reactive gas mixture. It was expected that, if the above postulation regarding the correlation between the ternary film microstructure evolution and its electrical properties is correct, an improvement of the electrical properties of the film would be achieved for the as-deposited TiN-P films grown from this gas mixture. Indeed, measuring the sheet resistivity of the films that were grown from the DMATi, H_2,NH_3 and TBP gas mixture showed much lower values. Films that were deposited at 350 °C had a resistivity of 2×10^3 $\mu\Omega$ cm (compared with 4×10^4 $\mu\Omega$ cm in the film that was deposited under the same conditions, but without adding TBP). Elevating the deposition temperature led to further reduction of the film sensitivity to a minimum of 2×10^2 $\mu\Omega$ cm for 500 °C.

Plots 2 and 3 in figure 6 exhibit the resistivity of films that were deposited from the gas mixture that included TBP, at temperatures of 350 and 400 °C, respectively, as a function of the post-deposition sintering temperature. As was observed in the previous films, applying a post-deposition heat treatment at elevated temperatures led, in these films, to a reduction of the film resistivity to a minimum value, regardless of the deposition temperature, of 35 $\mu\Omega$ cm as a result of heating at 550 °C. It is interesting to mention, however, that the higher the deposition temperature, the lower the initial resistivity value, and the higher the post-deposition temperature required to obtain the most significant resistivity reduction. Once again, for sintering temperatures above 600 °C, the reaction of the TiN film with the substrate was extensive, and the dry etch rates became zero.

The microstructure of these films deposited from the DMATi-NH_3-H_2-TBP gas mixture was studied by means of TEM. Figure 7 shows the TEM bright-field image (left side), dark-field image (right side) and the selected-area electron diffraction pattern of a film that was deposited from this gas mixture at a temperature of 350 °C (figure 7(*b*)). This film, and all the films that are discussed in this work, were deposited from the optimum gas mixture that comprises 25 SCCM DMATi, 1250 SCCM H_2 and 10 SCCM NH_3, at an approximate chamber pressure of 2.5 Torr. The film shown in figure 7(*b*) was deposited at 350 °C for 15 s and its TEM analysis is compared to a film that was deposited under exactly the same conditions, but without TBP in the gas mixture (figure 7(*a*)). This film was post-deposition sintered at 400 °C, and contained the newly formed, unidentified ternary phase, and thus its selected-area electron diffraction pattern reflects the existence of both the J FCC TiN_x phase and the new phase. One can see that both diffraction patterns (figures 7(*a*) and 7(*b*)) look similar, and

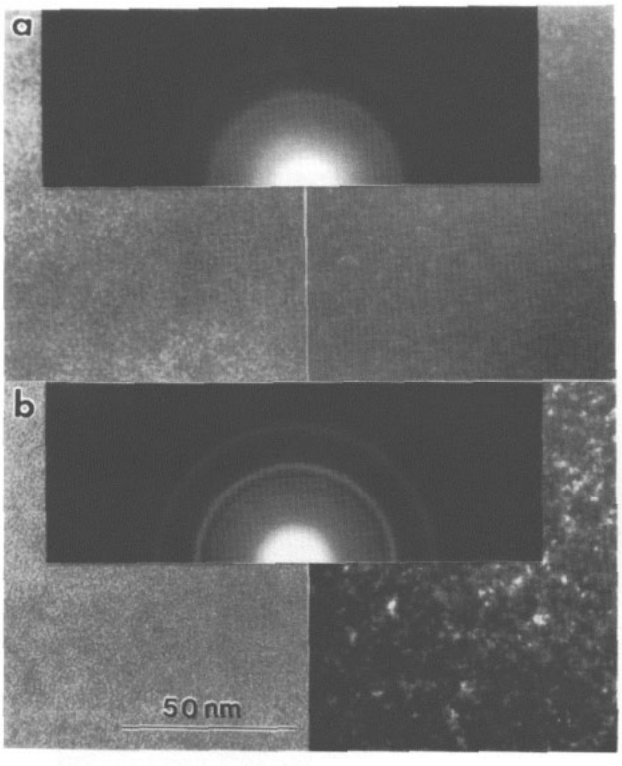

Figure 7. TEM plan-view bright-field (left) and centred dark-field (right) micrographs, as well as selected-area electron diffraction pattern of TiN_x films that were deposited onto InP substrates at 350 °C using a gas mixture of (*a*) DMATi–NH_3–H_2, and (*b*) DMATi–NH_3–H_2–TBP.

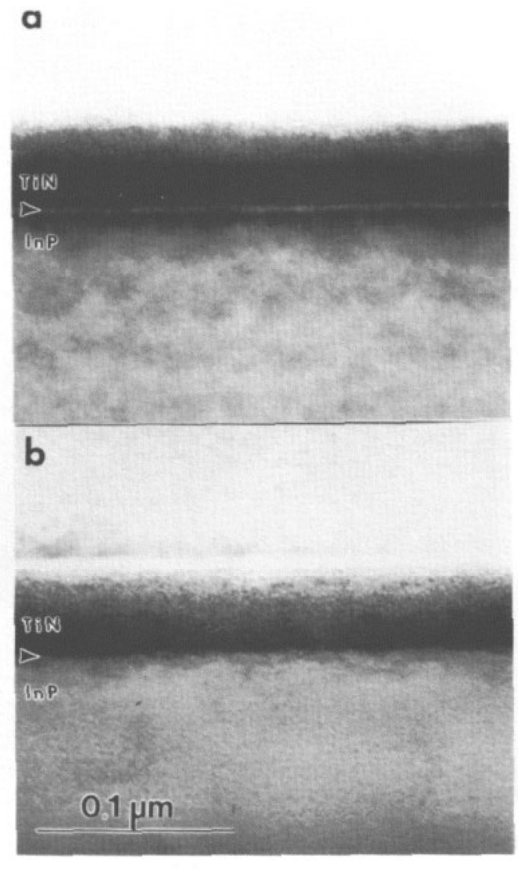

Figure 8. TEM cross-sectional images of TiN_x films that were deposited at 350 °C using gas mixtures of (*a*) DMATi–NH_3–H_2, and (*b*) DMATi–NH_3–H_2–TBP.

exhibit the same rings, which suggests the existence of the ternary Ti–N–P new phase in the film that was grown from the DMATi–NH_3–H_2–TBP, already as-deposited. AES data verified the incorporation of P in the TiN layer in the amount of approximately 3% atomic concentration.

Figure 8 provides TEM cross-sectional images of TiN_x films that were deposited at 350 °C for 15 s from a gas mixture comprising DMATi–NH_3–H_2 (figure 8(*a*)) and DMATi–NH_3–H_2–TBP (figure 8(*b*)). Both films, which were post-deposition sintered at 400 °C for 30 s, look similar, and in spite of the relatively high temperature of deposition and subsequential sintering, retain a small-grain polycrystalline microstructure. A thin interfacial reacted layer about 20 nm thick is observed at the TiN_x/InP interface when depositing the film from a P-free gas mixture (figure 8(*a*)). Since the TiN_x/InP interface in the latter sample (figure 8(*b*)) looks sharper, one can conclude that film that already contained P as-deposited reacted less with the InP through subsequent heat treatment. Furthermore, having the P incorporated into the film prior to the sintering provides an artificial P over-pressure over the InP substrate and suppresses the P out-diffusion. This apparently stabilizes the overall contact structure through subsequent aging and heat treatments.

Figure 9 provides TEM bright-field (left side) and dark-field (right side) images, as well as selected-area electron diffraction patterns of films that were deposited from a gas mixture that comprised TBP and which were subsequently sintered at various temperatures of 400 (figure 9(*a*)), 450 (figure 9(*b*)), 500 (figure 9(*c*)), and 550 °C (figure 9(*d*)). The higher the post-deposition sintering temperature, the lower the film resistivity, with a minimum of 35 $\mu\Omega$ cm as a result of heating at 550 °C. This suggests the existence of a larger amount of Ti–N–P low-resistance ternary phase in the deposited film. The selected-area electron diffraction of the sample that was sintered at 550 °C indeed showed another diffraction ring which is associated with this phase, as well as a thin layer of some clear preformed crystallographic grain. The size of the new phase grains, shown light in the dark-field images, does not change in an observable manner, however, as a result of the post-deposition sintering in the temperature range investigated.

Figure 10 gives the TEM cross-sectional micrographs of these samples. One can see that a post-deposition sintering at temperatures lower than 500 °C (figures 10(*a*) and 10(*b*)) led only to a very uniform and limited interfacial reaction between the deposited film and the InP substrate. Post-deposition sintering at 500 °C (figure 10(*c*)) led to clear nucleation and growth of larger grains at the interface, which grew even larger upon sintering at higher temperatures (figure 10(*d*)).

The influence of the deposition temperature on the quality of the film resistivity was evaluated earlier (figure

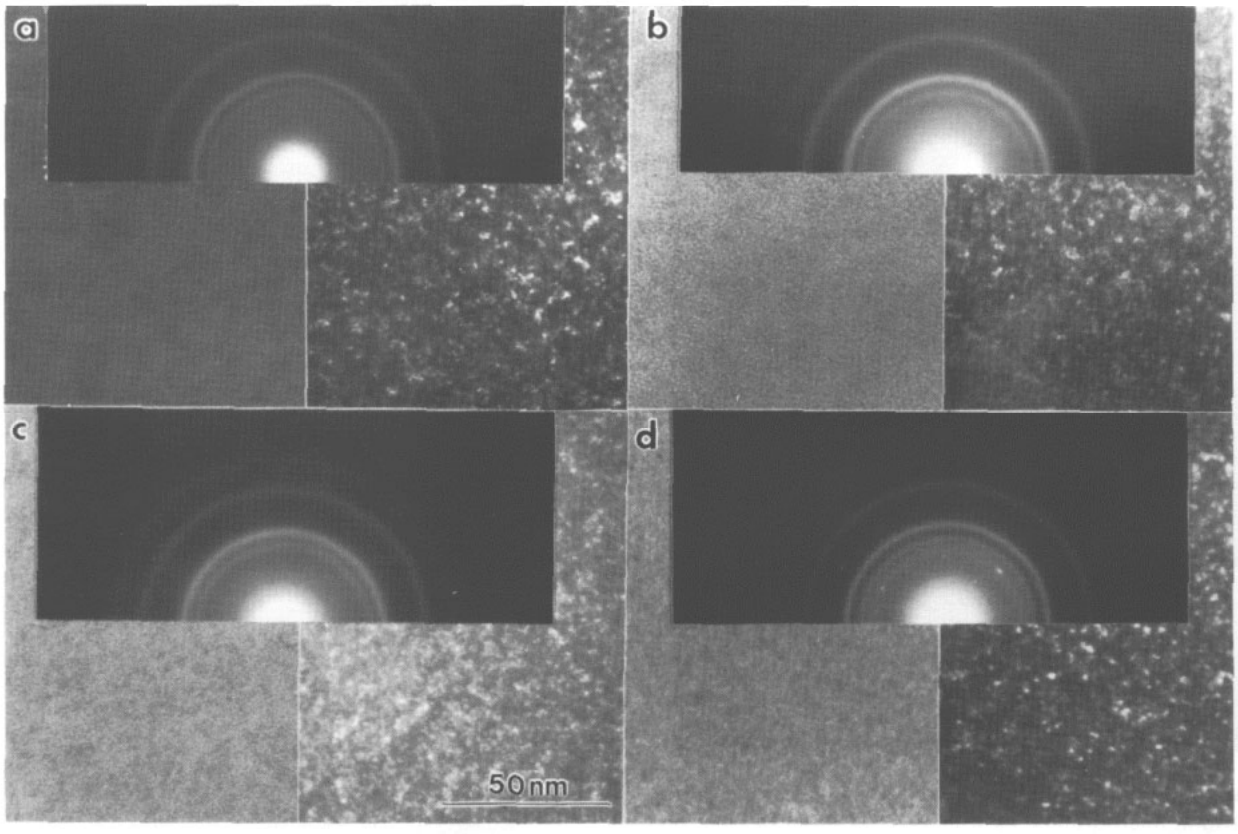

Figure 9. TEM plan-view bright-field (left) and centred dark-field (right) micrographs as well as selected-area electron diffraction patterns of TiN_x films that were deposited from a gas mixture of DMATi–NH_3–H_2–TBP at 350 °C and were subsequently sintered at (*a*) 400 °C, (*b*) 450 °C, (*c*) 500 °C and (*d*) 550 °C.

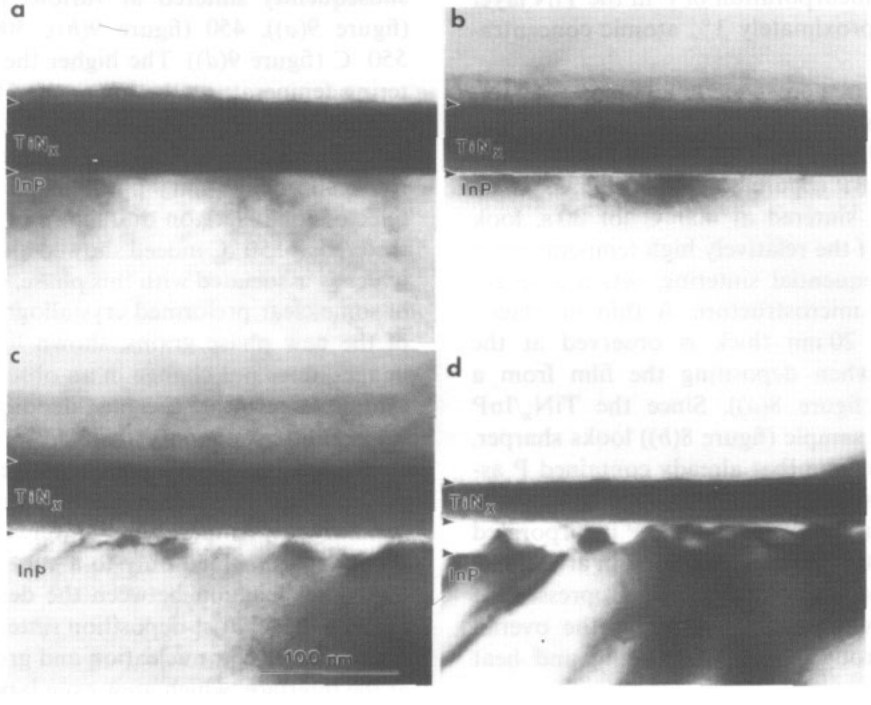

Figure 10. TEM cross-sectional images of TiN_x films that were deposited from a gas mixture of DMATi–NH_3–H_2–TBP at 350 °C and were subsequently sintered at (*a*) 400 °C, (*b*) 450 °C, (*c*) 500 °C and (*d*) 550 °C.

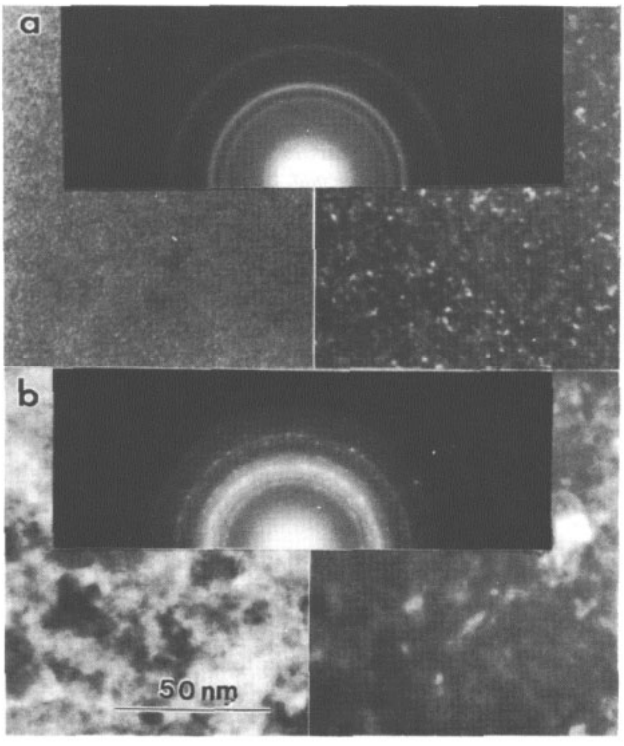

Figure 11. TEM plan-view bright-field (left) and centred dark-field (right) micrographs, as well as selected-area electron diffraction pattern of TiN_x films that were deposited from a gas mixture of DMATi–NH_3–H_2–TBP at (*a*) 400 °C and (*b*) 450 °C, and were subsequently sintered at 550 °C.

6) and showed a superior film behaviour for deposition at higher temperatures. Figure 11 shows TEM bright-field (left side) and dark-field (right side) images, as well as selected-area electron diffraction patterns of films that were deposited from the DMATi–NH_3–H_2–TBP gas mixture at 400 (figure 11(*a*)) and 450 °C (figure 11(*b*)) and were subsequently sintered at 550 °C. While the former films present similar microstructure and diffraction pattern to films deposited at a lower temperature, the latter show much larger grains clearly oriented in preferred crystallographic orientations. This film had the lowest measured film resistivity of 35 $\mu\Omega$ cm and the concentration of phosphorus was measured by AES to be about 5%.

Figure 12 shows a TEM cross-sectional micrograph of the sample that was deposited at 450 °C for 10 s and post-deposition sintered at 550 °C for 30 s. An almost continuous intermetallic layer (30 nm thick) was formed in between the deposited film and the InP substrate, consisting of columnar large grains, as was observed in the TEM plan-view analysis.

4. Summary and conclusions

We have demonstrated the formation of a very low-resistivity TiN_x–P film deposited onto InP substrates by means of the RT-LPMOCVD technique, using Tetrakis (dimethylamido) titanium and tertiarybutylphosphine

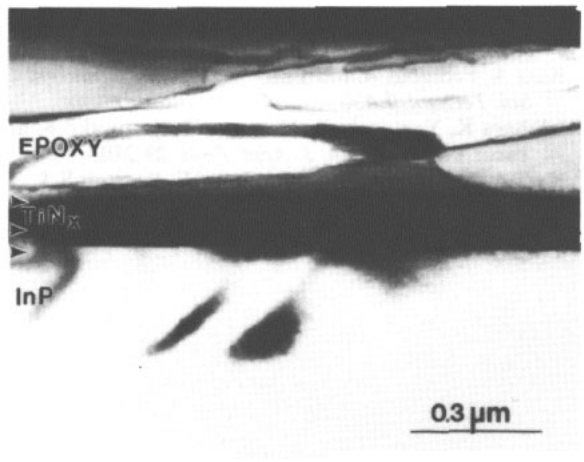

Figure 12. TEM cross-sectional image of a TiN_x film that was deposited from a gas mixture of DMATi–NH_3–H_2–TBP at 450 °C and was subsequently sintered at 550 °C.

(TBP) metalorganic liquid precursors as well as ammonia (NH_3) and hydrogen (H_2) in the reactive gas mixture and also by applying a post-deposition sintering process. As a result a new and as yet unidentified Ti–N–P ternary phase was formed, which has a crystal structure and lattice constant similar to the identified $Li_9TiN_3O_2$ phase. This phase was formed at the TiN_x film as a result of out-diffusion of phosphorus from the InP substrate for heating at temperatures of 400 °C or higher, and was formed in the as-deposited TiN_x–P film when TBP was present in the gas mixture. The formation of this phase led to a sharp reduction of the film resistivity to a minimum value of 35 $\mu\Omega$ cm for deposition of the TiN_x–P film at 400–450 °C and subsequently sintering at 550 °C. Further work is needed in order to define the crystallization structure of the new low-resistivity phase.

Acknowledgments

We are grateful to W C Dautremont-Smith, V D Mattera and S S Pei for supporting this work.

References

[1] Maeda T, Shima S, Nakayama T, Kakumu M, Mori K, Iwabuchi S, Aoki R and Matsunaga J 1985 *IEDM Tech. Digest* **85** 610
[2] Okamoto T, Shimizu M, Ohsaki A, Mashiko Y, Tsukamoto K, Matsukawa T and Nagao S 1987 *J. Appl. Phys.* **62** 4465
[3] Joshi R V, May D, Brodski S, Charari A, Krusin-Elbaum L, Restle P J, Nguyen T N and Oh C S 1989 *Appl. Phys. Lett.* **54** 1672
[4] Lichun Z and Yuzhi G 1989 *Chinese J. Semicond.* **10** 241
[5] Ting C Y 1982 *J. Vac. Sci. Technol.* **21** 14
[6] Musil J and Kadlec S 1990 *Vacuum* **40** 435
[7] Schintlmeister W, Pacher D and Pfaffinger K 1976 *J. Electrochem. Soc.* **123** 924
[8] Fix R M, Gordon R G and Hoffman D M 1990 *Chemical Vapor Deposition of Refractory Metals and*

Ceramics ed T M Besman and B M Gallois (Pittsburgh, PA: Materials Research Society) p 357
[9] Katz A, Feingold A and Pearton S J 1992 *Semicond. Sci. Technol.* **7** 436
[10] Ishihara K, Yamazaki K, Hamada H, Kamisako K and Tarui Y 1990 *Japan. J. Appl. Phys.* **29** 2103
[11] Katz A, Feingold A, Geva M, Lane E, Pearton S J, Ellington M and Chakrabarti U K 1991 *J. Appl. Phys.* **70** 1
[12] Katz A, Feingold A, Nakahara S, Lane E, Geva M, Pearton S J, Stevie F A and Jones K 1992 *J. Appl. Phys.* **71** 993
[13] Katz A, Feingold A, Pearton S J, Chakrabarti U K and Lee K M 1992 *Semicond. Sci. Technol.* **7** 583